IEEE Access
Multidisciplinary | Rapid Review | Open Access Journal

Received June 12, 2019, accepted July 11, 2019, date of publication July 19, 2019, date of current version October 4, 2019.

Digital Object Identifier 10.1109/ACCESS.2019.2930047

Research on High Efficiency V/f Control of Segment Winding Permanent Magnet Linear Synchronous Motor

LEILEI CUI, HONGWEI ZHANG, AND DI JIANG
School of Electrical Engineering and Automation, Henan Polytechnic University, Jiaozuo 454000, China
Corresponding author: Hongwei Zhang (zhanghw@hpu.edu.cn)

This work was supported by the Natural Science Foundation of Henan Province, China, under Grant 162300410349.

ABSTRACT By analyzing the relationship between the electromagnetic parameters and the secondary position during the primary and secondary coupling transition of the segment winding permanent magnet linear synchronous motor (SW-PMLSM), the variable parameter mathematical model of the rotor side of the SW-PMLSM is established. Taking the three-stage primary lifting system as an example, the dynamic process of the whole system is simulated and analyzed. According to the characteristics of its parameters, the segmentation vector control is obtained as the best stability control method. However, in practical applications, in order to save costs, the segmented linear motor often adopts the effective section parallel power supply mode, and the SW-PMLSM parallel power supply model is obtained by approximate simplification. This paper proposes a SW-PMLSM high-efficiency V/f control method, which combines the advantages of traditional V/f control and field-oriented control. It does not need to install position sensor, and can realize simple and high-performance motor drive. Finally, simulation and experimental results are provided to validate the effectiveness of the fidelity of the proposed strategy.

INDEX TERMS SW-PMLSM, vector control, effective segment parallel power supply, variable parameter mathematical model, simulation modeling, efficient V/f control.

I. INTRODUCTION

As a new type of linear motor, the primary segment winding permanent magnet linear synchronous motor has the advantages of high thrust density, low power loss and fast dynamic response [1]–[4]. It is an ideal driving source for cordless lifting systems and has outstanding advantages in ultra-deep mine upgrading, super high-rise buildings and shipboard lifts. And the moving secondary structure does not require the drive cable to move with the secondary, and the permanent magnet can also be effectively protected, at the same time, it solves the problems of the stator magnetic resistance, the excessive inductance, the high driving voltage, the large electromagnetic loss and the low overall efficiency caused by the excessively long primary magnetic steel linear motor. The modular primary segmentation structure also has the advantages of flexible topology, easy manufacturing, easy maintenance and many other advantages. The primary length and secondary length of the primary segmented motor and the gap between the primary segments can be determined according to the actual application, control accuracy requirements, cost and reliability. In order to ensure that the electromagnetic thrust of the motor output during the dynamic movement of the stator between the stators is stable and has a smaller end effect, the segmented motor is usually designed as a segment between the primary windings and the primary core is not segmented. Segment winding permanent magnet linear synchronous motor (SW-PMLSM) with no gap structure between segments. Research has shown that [5]–[9], this structure can effectively reduce the thrust fluctuation during the operation between the primary sections, and is suitable for places where the thrust stability is required.

Accurate mathematical model is the basis for drive controller design and system performance analysis. In the primary segmented permanent magnet linear motor, in addition to the end effect problem, there is a special magnetic field phenomenon such as a half-opening threshold uncoupled magnetic field between the primary and secondary, and an

The associate editor coordinating the review of this manuscript and approving it for publication was Engang Tian.

excessive dynamic magnetic field between the secondary segments. Therefore, the parameter characteristics in its mathematical model are different from ordinary synchronous motors. It is necessary to study the key electromagnetic parameters in the mathematical model of the motor in combination with specific topological structures and inter-segment transitions. Establishing an accurate simulation model that is closer to the actual physical state and has realistic engineering achievability is of great significance for motor performance optimization and control research, and facilitates united simulation of motor and system [10]–[12].

Since the research on "SW-PMLSM vertical lifting system", the Institute of Electrical Application of Henan Polytechnic University has made great progress in solving magnetic field, analyzing and calculating magnetic field characteristics [13]–[18], At present, the laboratory has built the most advanced "SW-PMLSM industrial testing machine model " in China.

Since the SW-PMLSM is a long-stroke laying installation, position data acquisition on the motor mover side becomes quite difficult. The traditional V/f control does not need to add a position sensor to detect the position of the mover, and its control mode is relatively simple. It is a low-cost implementation method in the sensorless control method, and is often applied to a permanent magnet synchronous motor with a damper winding. However, for ordinary permanent magnet synchronous motors, the damping effect of asynchronous torque on torque ripple is lacking, which makes the adaptability of the motor to the load during operation worse, and it is easy to lose the step under the system disturbance. In addition, the conventional V/f control is different from the current vector control in that it cannot achieve an efficient and stable control effect like current vector control [19]–[24].

The active reactive power of the motor is calculated by the current detected on the stator side, and the proportional gain is introduced into the closed loop to compensate the input voltage amplitude and phase angle (electromagnetic field rotational speed) of the stator in the V/f control. This closed-loop V/f control avoids the introduction of complex operations brought by vector control and achieves efficiency control.

II. MODEL OF SW-PMLSM

Different from the traditional PMLSM, the magnetic circuit structure between the primary and secondary of the SW-PMLSM changes with the relative position, so the electromagnetic parameters of the motor are a function of the secondary position. When considering the influence of magnetic saturation, some electromagnetic parameters are also a function of armature current, which has strong nonlinear characteristics. Numerical analysis is usually used to solve the relationship between these parameters and secondary position and current (for simplicity, this article ignores the influence of magnetic circuit saturation). It can be seen that finding the nonlinear and variable parametric magnetic circuit relationship of SW-PMLSM is a key issue in overall modeling.

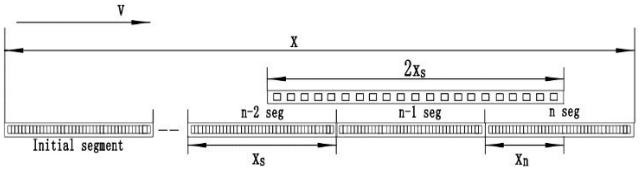

FIGURE 1. SW-PMLSM structure diagram.

A. THE VARIATION LAW AND ANALYSIS OF ELECTROMAGNETIC PARAMETERS OF SW-PMLSM

The research object of this paper is SW-PMLSM with winding segmentation, no gap structure between segments, and the length of the mover is a multiple of the single-segment stator (The thrust of each section of the SW-PMLSM with this structure is uniformly changed during the winding switching process). The SW-PMLSM structure is shown in Figure 1. The primary winding is a closely spaced topology with a secondary length that is twice the length of a single-stage primary winding. During the operation of the motor, the magnetic field coupling relationship between the primary and secondary has the following four conditions:

(1) The mover permanent magnet is not within the excitation magnetic field of the unit stator winding (inactive segment).

(2) The mover permanent magnet gradually enters the excitation field of the unit stator winding (effective segment N).

(3) The permanent magnet of the mover is fully coupled to the excitation field of the stator winding of the unit (effective segment $N-1$).

(4) The mover permanent magnet gradually exits the excitation magnetic field range of the unit stator winding (effective segment $N-2$).

In the SW-PMLSM operation, the switching of the effective segment is a process of connecting, and the SW-PMLSM can be equivalent to the effective operation of three linear motors placed together.

B. VARIATION RULE OF SYNCHRONOUS INDUCTANCE PARAMETERS

During the actual operation of SW-PMLSM, the actual coupling degree of the three-phase winding and the mover is related to the position of the mover, and there is a semi-filled groove at the end of each section of the primary winding, so the three-phase inductance of the three-phase winding is asymmetrical and is a function of the secondary position.

The calculation formula of the permanent magnet linear synchronous motor cross-axis inductance is:

$$\begin{cases} L_d = L_{s0} + \mathrm{M}_{s0} + 1.5L_{s2} \\ L_q = L_{s0} + \mathrm{M}_{s0} - 1.5L_{s2} \end{cases} \tag{1}$$

In the formula: L_{s0}, L_{s2}, M_{s0} are the average of the self-inductance, the secondary component of the self-inductance, and the average of the mutual inductance.

Taking the A-phase winding as an example, the self-inductance of the A-phase winding of a conventional permanent magnet linear motor can be obtained according to the definition of inductance and the double-reaction theory.

$$L_{AA} = L_{s0} + L_{s2}\cos 2\frac{\pi}{\tau}x \tag{2}$$

$$\begin{cases} L_{s0} = L_{A\sigma} + L_{m1} \\ L_{s2} = \dfrac{1}{2}L_{m1} \end{cases} \tag{3}$$

$L_{A\sigma}$ and L_{m1} are the leakage magnetic self-inductance and excitation self-inductance of the phase winding.

Considering that the SW-PMLSM prototype is surface-mount, the self-inductance secondary component is very small, so only the variation law of the average value of the phase self-inductance is considered. When the mover exits a certain stator, the air gap between the primary and secondary is gradually Increase, the proportion of leakage inductance increases, when the mover completely withdraws, the self-inductance is completely composed of leakage inductance. Similarly, the mutual component secondary component is not considered. When the mover exits a certain stator, the air gap permeability decreases gradually, and the mutual inductance average decreases with the mover position. Therefore, the expression of the cross-axis inductance between the motor segments can be simplified as:

$$L_s = L_d = L_q = L_{s0}(x) + M_{s0}(x) \tag{4}$$

The synchronous linear inductance of the motor's cross-axis is approximately linear with the position of the mover. The law can be expressed as:

$$L_s(x) = L_{s\sigma} + L_m \cdot \frac{x_s}{x_n} \tag{5}$$

Among them: $L_{s\sigma}$ is the leakage inductance, $L_m(x)$ is the equivalent excitation inductance, x_n is the segment coupling length, x_s is the effective coupling length.

C. VARIATION LAW AND MODELING OF PERMANENT MAGNET COUPLED FLUX OF SW-PMLSM

The permanent magnet coupled flux linkage is the function of the permanent magnet to the stator winding of each phase, and is also the key parameter for establishing the mathematical model of the permanent magnet linear synchronous motor rotating coordinate system. The permanent magnet coupled flux linkage of each phase winding of PMLSM is

$$\begin{cases} \psi_{fA} = \psi_f(x) \cdot \cos(\dfrac{\pi}{\tau} \cdot x) \\ \psi_{fB} = \psi_f(x) \cdot \cos(\dfrac{\pi}{\tau} \cdot x - \dfrac{2}{3}\pi) \\ \psi_{fC} = \psi_f(x) \cdot \cos(\dfrac{\pi}{\tau} \cdot x + \dfrac{2}{3}\pi) \end{cases} \tag{6}$$

For SW-PMLSM, when the coupling area between the primary and secondary remains unchanged, the amplitude of the coupled magnetic flux of the permanent magnet is constant, and the size of the permanent magnet coupled flux changes with the coupling area between the primary and secondary When the mover gradually withdraws from a certain stator section, the permanent magnet coupled flux linkage is gradually reduced to zero, and its variation can be regarded as a linear change in the approximate analysis. The vector form can be expressed as:

$$\psi_f(x) = \psi_{f\,\max} \cdot \frac{x_n}{x_s} \cdot e^{j\frac{\pi}{\tau}x} \tag{7}$$

Among them: $\psi_{f\,\max}$ is the permanent magnet flux linkage change amplitude, x_n is the segment length, x_s is the effective coupling length.

D. VARIABL PARAMETER MATHEMATICAL MODEL OF SW-PMLSM

The mathematical model of SW-PMLSM is similar to the mathematical model of traditional PMLSM, but the influence of the change of the position of the mover on the electromagnetic parameters of the motor needs to be considered. The specific performance is that the model of SW-PMLSM is a mathematical model of variable parameters related to the position of the mover.

The mathematical model of SW-PMLSM in the stator ABC phase coordinate system can be expressed as

$$\text{Voltage equation}: \begin{cases} u_A = R_S \cdot i_A + \dfrac{d\psi_A(x)}{dt} \\ u_B = R_S \cdot i_B + \dfrac{d\psi_B(x)}{dt} \\ u_C = R_S \cdot i_C + \dfrac{d\psi_C(x)}{dt} \end{cases} \tag{8}$$

Magnetic chain equation:

$$\begin{cases} \psi_A = L_{AA}(x) \cdot i_A + M_{AB}(x) \cdot i_B \\ +M_{AC}(x) \cdot i_C + \psi_{fA}(x) \\ \psi_B = M_{BA}(x) \cdot i_A + L_{BB}(x) \cdot i_B \\ +M_{BC}(x) \cdot i_C + \psi_{fB}(x) \\ \psi_C = M_{CA}(x) \cdot i_A \\ +M_{CB}(x) \cdot i_B + L_{CC}(x) \cdot i_C + \psi_{fC}(x) \end{cases} \tag{9}$$

It can be obtained by the combination of (8) and (9):

(x) represent the position of the secondary and p represents the differential operator for time t. The inductance matrix and the permanent magnet interaction flux are functions of the position of the mover x, so

$$\begin{cases} p\psi(x) = \dfrac{d\psi(x)}{dx} \cdot \dfrac{dx}{dt} = v \cdot p_x\psi(x) \\ pL(x) = \dfrac{dL(x)}{dx} \cdot \dfrac{dx}{dt} = v \cdot p_xL(x) \end{cases} \tag{11}$$

$L(x)$ and $\psi(x)$ are the inductance and flux chain matrix respectively, p_x is the differential operator for the position of the mover x.

$$\begin{bmatrix} u_A \\ u_B \\ u_C \end{bmatrix} = \begin{bmatrix} R_s & 0 & 0 \\ 0 & R_s & 0 \\ 0 & 0 & R_s \end{bmatrix} \cdot \begin{bmatrix} i_A \\ i_B \\ i_C \end{bmatrix} + v \cdot \left(p_x \begin{bmatrix} L_{AA}(x) & M_{AB}(x) & M_{AC}(x) \\ M_{BA}(x) & L_{BB}(x) & M_{BC}(x) \\ M_{CA}(x) & M_{CB}(x) & L_{CC}(x) \end{bmatrix} \right) \cdot \begin{bmatrix} i_A \\ i_B \\ i_C \end{bmatrix} + \begin{bmatrix} L_{AA}(x) & M_{AB}(x) & M_{AC}(x) \\ M_{BA}(x) & L_{BB}(x) & M_{BC}(x) \\ M_{CA}(x) & M_{CB}(x) & L_{CC}(x) \end{bmatrix} \cdot \left(p \begin{bmatrix} i_A \\ i_B \\ i_C \end{bmatrix} \right) + v \cdot \left(p_x \begin{bmatrix} \psi_f \cdot \cos(\frac{\pi}{\tau} \cdot x) \\ \psi_f \cdot \cos(\frac{\pi}{\tau} \cdot x - \frac{2}{3}\pi) \\ \psi_f \cdot \cos(\frac{\pi}{\tau} \cdot x + \frac{2}{3}\pi) \end{bmatrix} \right) \tag{10}$$

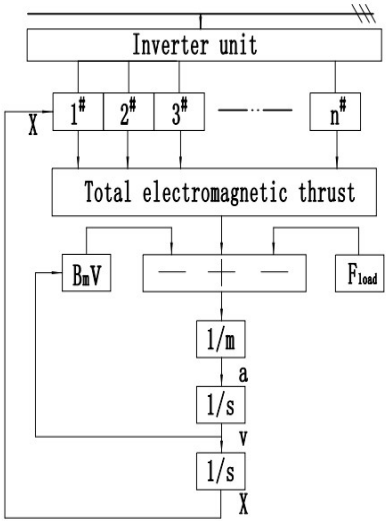

FIGURE 2. SW-PMLSM overall block diagram.

The mathematical model of SW-PMLSM in the rotating coordinate system obtained by coordinate transformation is:

$$\begin{cases} u_d = R_s \cdot i_d + v \cdot p_x \psi_f(x) + v \cdot p_x L_s(x) \cdot i_d \\ +L_s(x) \cdot p i_d - v \cdot \frac{\pi}{\tau} \cdot L_s(x) \cdot i_q \\ u_q = R_s \cdot i_q + v \cdot p_x L_s(x) \cdot i_q + L_s(x) \cdot p i_q \\ +v \cdot \frac{\pi}{\tau} \cdot \left[L_s(x) \cdot i_d + \psi_f(x) \right] \end{cases} \tag{12}$$

$L_s(x)$ is a straight-axis synchronous inductor, $\psi_f(x)$ is a permanent magnet coupled flux linkage.

E. THE OVERALL MODEL OF SW-PMLSM

Electromagnetic thrust equation in d-q synchronous coordinate system:

$$F_e = \frac{3}{2} \cdot P_n \cdot \frac{\pi}{\tau} \cdot \left[\psi_f \cdot i_q + (L_d - L_q) \cdot i_d \cdot i_q \right] \tag{13}$$

The overall block diagram of the winding segmented permanent magnet linear synchronous motor is shown in Figure 2. For SW-PMLSM with n segments in power supply, the magnetic resistance is ignored and the total mechanical motion equation can be expressed as:

$$\begin{cases} m \dfrac{d^2x}{dt^2} = \sum F_e(x) - mg \pm B_m v \\ \sum F_e(x) = \sum_{k=1}^{n} F_{ek}(x) \end{cases} \tag{14}$$

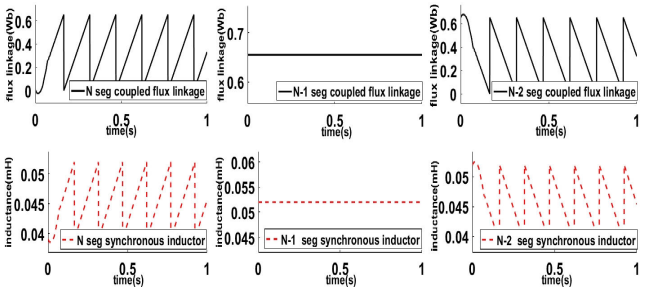

FIGURE 3. Periodic diagram of stator parameters of effective action section.

m is the weight of the mover, B_m is friction damping coefficient and $F_e(x)$ is the sum of electromagnetic thrust.

III. ESTABLISHMENT AND ANALYSIS OF SIMULATION MODELS

Simulation model analysis: The SW-PMLSM mover length studied in this paper is twice the length of a single-segment stator. At any time, it is necessary to meet the three-stage stator armature in the power supply state. One of the stator windings of the motor is fully coupled with the mover, one segment of the stator winding is in the state of the mover gradually entering, and the other is in the state of the mover gradually exiting the stator segment (the stator segment that is not coupled with the electric field of the mover is ignored).These three states are always present during the actual linear operation of the segmented motor. The n segment is always defined as the front segment where the initial and secondary coupling motions occur, and the n segment is always in the state where the mover gradually enters, and the initial and secondary inductance parameters and the permanent magnet flux linkage parameters increase with the coupling area. Increase, when the maximum value is reached, it is adjusted to re-enter with the definition of the front end. With the change of the displacement x, the parameters of the n-segment stator periodically change, and the n-1 segment and the n-2 segment are defined as the first and second segments. The middle and the end of the stator where the stage coupling occurs. The inductance parameters of the three-stage stator and the magnetic flux linkage parameters of the permanent magnets appear as shown in Fig.3.

A. SW-PMLSM PARALLEL POWER SUPPLY OPEN-LOOP V/F CONTROL

The traditional open-loop V/f control is the most easy to implement control method in the industrial field, and the most control method to test the basic properties of the controlled object. The pole distance of the simulation prototype is set to 22.5mm, the control mode is V/f open loop control, the segmented stator power supply mode is segmented parallel power supply, the phase voltage of the three-phase power supply is set to 380v, and the power supply frequency is 33hz. The linear speed of the motor is $v = 2\tau f$.Since the set power frequency is low, the linear line speed is small and it can be started directly. At time t=0, the load weight is set to 500 kg. The dynamic characteristics corresponding to the valid segment of the stator are shown in the figure below.

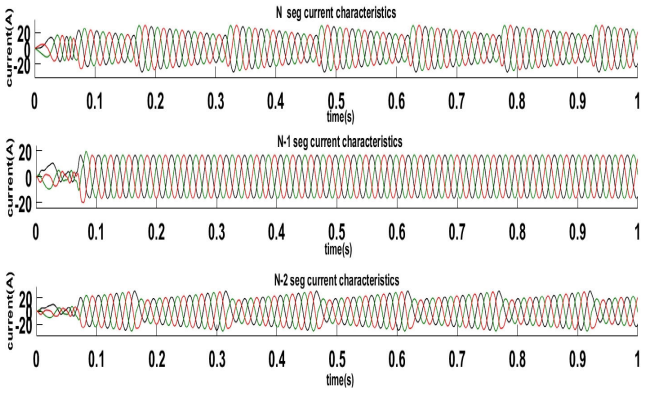

FIGURE 4. Dynamic characteristics of stator current in effective action section.

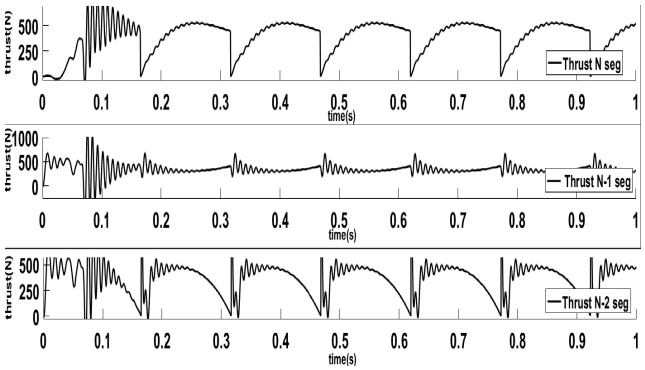

FIGURE 5. Dynamic characteristics of stator thrust in effective action section.

It can be seen from the above diagram that the stator three-phase current and the stator acting thrust of the segment of the segmented motor exhibit periodic changes, as shown by the change of position, the current of the n-segment stator with the inductance and flux linkage parameters. Increase and decrease (the supply voltage does not change), the electromagnetic thrust of the n-segment gradually increases due to the increase of the effective section of the coupling with

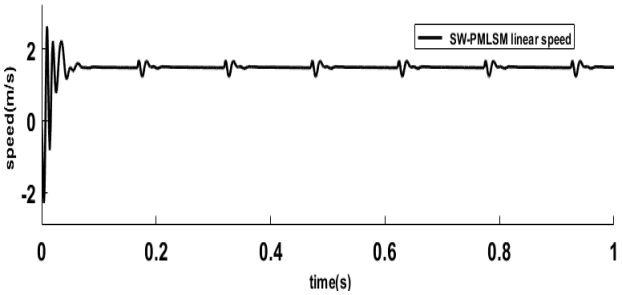

FIGURE 6. Linear motor linear speed dynamic characteristic diagram.

the secondary, and the n-2 segment stator is opposite to the n-segment stator, n-1 segment the electromagnetic thrust generated by the stator remains substantially unchanged. The resultant thrust gradually stabilizes as the speed pulsation slows down, and the system has a larger pulsation when switching between each segment (It should be noted that in the actual operation, the definition switching of the effective segment is a smooth transition process, and the stepping link is inevitably introduced when establishing the simulation model, so the simulation model reference only needs to observe the smooth interval feature).

B. SEGMENTED POWER SUPPLY VECTOR CURRENT CONTROL STRATEGY FOR SW-PMLSM

During the operation of SW-PMLSM, in order to achieve stable operation of the thrust, the following two conditions must be met:

1. $\psi_{f_n}(x) + \psi_{f_{n-2}}(x) = \psi_{f_{n-1}}(x)$, the length of the mover is an integer multiple of the length of the single-segment stator (SW-PMLSM for the segmented core without segmentation).

2. $i_{q_n} = i_{q_{n-1}} = i_{q_{n-2}}$, that is, the equivalent primary axis currents of the effective primary segments remain equal.

Meet 1, 2, in the entire operation of the segmented motor, always meet $F_{e_{\text{total}}} = 2 \cdot F_{e_{n-1}} = F_{e_n} + F_{e_{n-2}}$, the thrust and speed remain stable.

The direct thrust control of the conventional PMLSM is based on the adjustment of the thrust angle to maintain the thrust. The above analysis can be used to define the SW-PMLSM. On the basis of conditions above, the vector control strategy with current loop is a SW-PMLSM thrust stability control strategy.

The conventional current hysteresis vector control strategy is selected, and the SW-PMLSM is simulated by the inverter unit power supply. The specific control strategy is shown in the following figure:

At t=0, the load is set to 500KG. At t=0.5s, the load is suddenly increased to 1000KG. The dynamic simulation characteristics of the corresponding system-related parameters are as follows:

It can be seen from the above simulation results that the use of the segmented supply current hysteresis vector control strategy can effectively reduce the thrust fluctuations, enable the segmented motor to run more smoothly, and can quickly

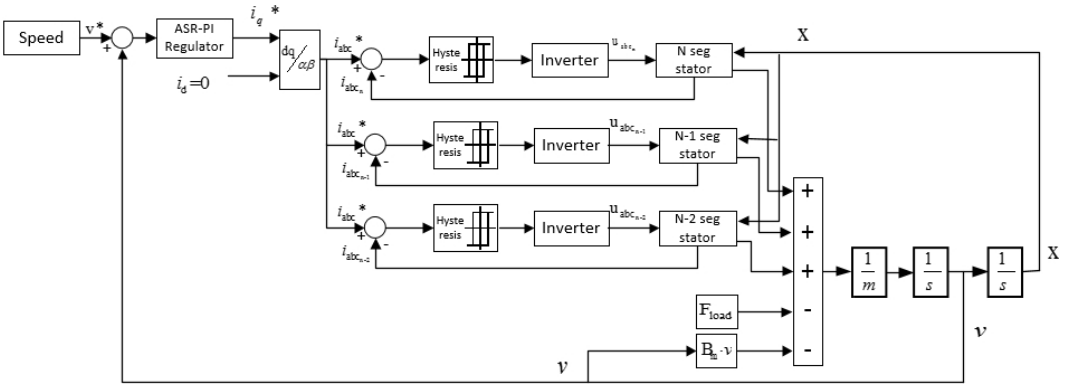

FIGURE 7. Segmented power supply current vector control strategy of SW-PMLSM.

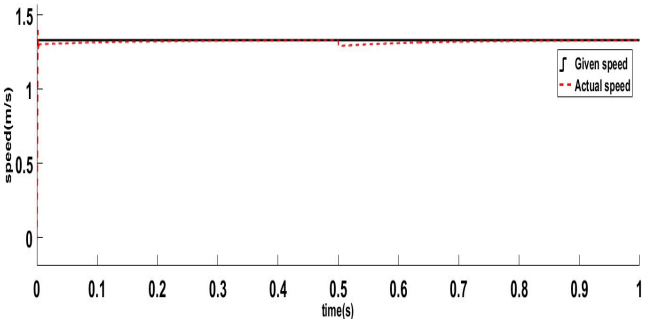

FIGURE 8. Segmented vector controlled speed curve.

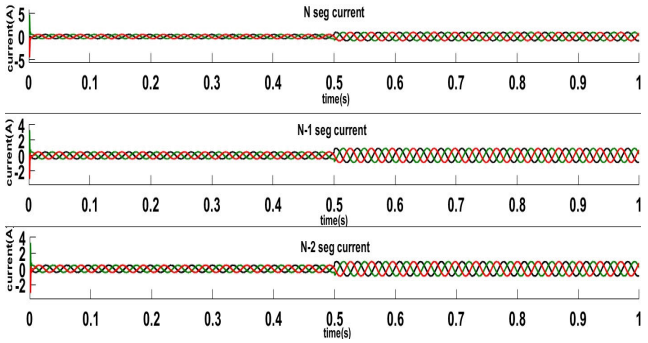

FIGURE 9. Segmented vector controlled current curve.

recover the previous motion state when the load is abrupt, and the system is very robust.

IV. RESEARCH ON SW-PMLSM HIGH EFFICIENCY V/F CONTROL

Although the segmented supply current hysteresis vector control method can achieve good control effects, the separate controllers in each segment undoubtedly increase the cost of the system. In normal system power supply, segmented power supply also increases the difficulty of control. In this case, it is necessary to study the stable operation control of SW-PMLSM in parallel power supply. In the design of the long-stroke SW-PMLSM, we usually use a single-supply effective section to supply power in parallel in order to save costs.

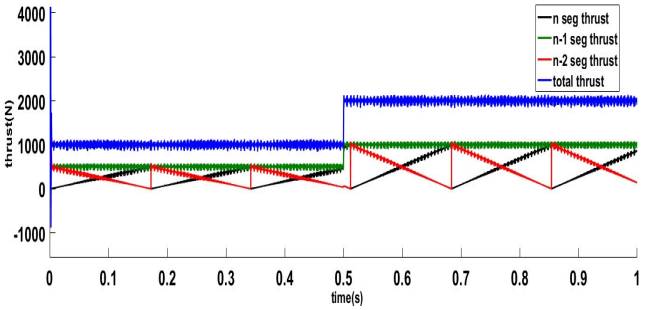

FIGURE 10. Segmented vector controlled thrust curve.

A. OVERALL MODELING OF SW-PMLSM PARALLEL POWER SUPPLY

From the perspective of segmentation, the overall model of the motor is actually the set of functions of each segment of the motor. The mathematical model of each valid segment of SW-PMLSM in the rotating coordinate system can be expressed as:

$$\begin{cases} \mathrm{u_{d\,x}} = \mathrm{R_s} \cdot i_{d\,x} + \dfrac{d}{dt}\left(\psi_{f\,x}(x) + L_{s\,x}(x) \cdot i_{d\,\mathrm{x}}\right) \\ -v \cdot \dfrac{\pi}{\tau} \cdot L_{s\,\mathrm{x}}(x) \cdot i_{q\,\mathrm{x}} \\ \mathrm{u_{q\,x}} = \mathrm{R_s} \cdot i_{q\,x} + \dfrac{d}{dt}\left(L_{s\,x}(x) \cdot i_{q\,\mathrm{x}}\right) \\ +v \cdot \dfrac{\pi}{\tau}\left[\psi_{f\,x}(x) + L_{s\,x}(x) \cdot i_{d\,\mathrm{x}}\right] \end{cases} \tag{15}$$

In fact, the value of the leakage inductance is much larger than the value of the equivalent magnetizing inductance. Therefore, the approximate dq axis voltage formula for parallel power supply is:

$$\begin{cases} 3u_d = R_s i_d + L_s \cdot \dfrac{di_d}{dt} - \omega \cdot L_s \cdot i_q \\ 3u_q = R_s i_q + L_s \cdot \dfrac{di_q}{dt} + \omega \cdot L_s \cdot i_d + 2\omega \cdot \psi_f \end{cases} \tag{16}$$

If the number of coupling segments is greater than one segment, assume that the number of coupling segments is m

segments:

$$\begin{cases} (m+2)\,u_d = R_s i_d + L_s \cdot \dfrac{di_d}{dt} - \omega \cdot L_s \cdot i_q \\ (m+2)\,u_q = R_s i_q + L_s \cdot \dfrac{di_q}{dt} + \omega \cdot L_s \cdot i_d \\ \quad + (m+1)\,\omega \cdot \psi_f \end{cases} \tag{17}$$

B. SW-PMLSM EFFICIENT V/F CONTROL STRATEGY

Traditional open-loop V/f control is a low-cost sensorless control implementation. This control method has poor adaptability to the load and is prone to out-of-step under disturbance. In addition, traditional open-loop V/f control does not achieve high efficiency control like vector control. In order to improve this situation, efficient closed-loop V/f control came into being. In this paper, a stable and efficient V/f control method is proposed. Two closed-loop feedback structures are designed. One is to adjust the phase angle of the input vector voltage based on the active power variation, called the stability loop. The second is to adjust the amplitude of the input vector voltage based on the unit current maximum torque (MTPA) target, called the efficiency loop.

The control block diagram is shown below:

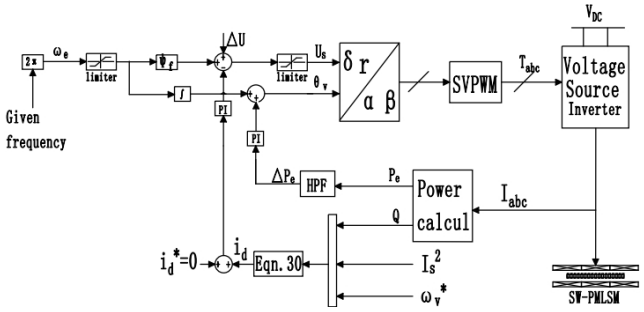

FIGURE 11. SW-PMLSM servo control system block diagram.

C. V/F STABLE RING DESIGN ANALYSIS

The motor's stabilizing ring is designed to design a damping ring similar to reduce motor speed fluctuations to improve its operating characteristics. The figure below shows the voltage and current vector diagram of the motor running. Where ω_u is the rotational speed of a given voltage command, θ_u is the angle between the voltage vector and the α axis, and the stability condition between the given voltage vector and the rotor is:

$$\omega_u = \omega_r + \Delta\omega_r \tag{18}$$

When an external disturbance occurs during operation, the mover will have a fluctuation of $\Delta\omega_r$ speed. In order to stabilize the system after the speed fluctuation, the given voltage vector will be adjusted during the transient process to avoid out-of-step.

Since the V/f control is a sensorless control, it is impossible to directly observe the fluctuation of the rotational speed of the electrode, and it can only be estimated by other means. The small-signal analysis method is used to analyze the dynamic equation of SW-PMLSM (for the sake of understanding, the rotation quantity is still used for analysis), and the mechanical motion small-signal model can be obtained as follows:

$$\Delta\dot{\omega}_r = \frac{\Delta T_e}{J} - \frac{\Delta T_l}{J} - \frac{B}{J} \cdot \Delta\omega_r \tag{19}$$

It can be seen from the figure that the key to the stable design of the V/f control is that after the rotor side speed fluctuation is generated, the input vector voltage is compensated in time to avoid the loss of control.

The general electromagnetic torque equation for synchronous motors is:

$$T_e = \frac{3U_\delta E}{\omega_r L_d} \sin\delta + \frac{3U_\delta^2 (L_d - L_q)}{2\omega_r L_d L_q} \sin 2\delta \tag{20}$$

where: U_δ is the amplitude of the input voltage command, E is the induced voltage of the rotor magnetic motive force on the stator winding, and δ is the torque angle.

It can be deduced from equations (19) and (20) that the stability adjustment of V/f is to adjust ΔT_e by introducing two adjustment amounts δ and U_δ, so that $\Delta\omega_r$ tends to zero, thereby achieving system stability adjustment.

In the transient analysis, the power loss and the energy storage rate can be regarded as constant quantities. The average rotor power during transient disturbance can be expressed by the following equation:

$$\Delta P_e = \frac{4J\omega_0}{P_n^2} \cdot \frac{d}{dt}\Delta\omega_r + \frac{8}{P_n^2} B_m \omega_0 \Delta\omega_r + \frac{2}{P_n} T_{l0} \Delta\omega_r \tag{21}$$

where: ω_0 is the steady state speed different from the transient state, and T_{l0} is the steady state load torque.

That is, the fluctuation amount of the input power ΔP_e can characterize the rotational speed fluctuation $\Delta\omega_r$ of the rotor under the disturbance. ΔP_e is a high frequency component obtained after the active power is filtered by a high pass filter (HPF). The speed fluctuation can be estimated by:

$$H(s) = Ts/(Ts+1) \tag{22}$$

$$\Delta\omega_r = {-K_p}/{\omega_r^*} \cdot HPF(P_e) \tag{23}$$

The selection of the time constant T and the proportionality factor K_p is experimentally determined.

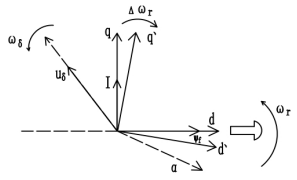

FIGURE 12. Motor running vector diagram.

For SW-PMLSM, the sum of the powers of the effective segments is equal to the combined power of each valid segment, satisfying the superposition theorem (discussed by other articles).

D. V/F EFFICIENCY LOOP DESIGN ANALYSIS

The synchronous motor can achieve high-efficiency operation state through different control methods. In this paper, the maximum torque per ampere (MTPA) is selected as the operation target. Implementing MTPA in current vector control is achieved by adjusting the angle between the current vector and the rotating coordinate axis. In V/f control, the rotor position is uncertain and cannot be directly controlled by this angle. Therefore, we construct an observation variable with MTPA control target, and achieve the purpose of MTPA control by adjusting the system parameters to achieve this observation target.

In order to obtain a larger power factor and higher efficiency using a minimum of permanent magnets, a permanent magnet synchronous motor is generally designed with a power factor hysteresis state of excessive demagnetization. As shown below:

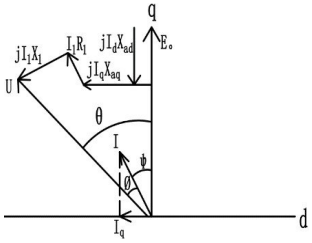

FIGURE 13. Permanent magnet synchronous motor vector.

After the permanent magnet motor is manufactured, the excitation cannot be adjusted, and the reactive power and power factor can be adjusted by adjusting the supply voltage. Assume that the perpendicular magnetic reluctance is equal, the stator voltage is ignored, and the load torque is constant (the output power is constant):

$$P_{em} = \frac{mUE_0}{X_s}\sin\theta = m\,UI_1\cos\varphi = C \tag{24}$$

When adjusting $\dot{U}$, the end point of $\dot{U}$ always falls on the perpendicular line AB parallel to $\dot{E}$ ($U\sin\theta = C_1$), and the end point of $\dot{I}$ falls on the curve CD ($\dot{I}\cos\varphi = {}^{C_2}/_{U}$). When the applied voltage changes, the current changes from the leading edge to the lag, and the power factor changes. The specific changes are shown in the figure14 below.

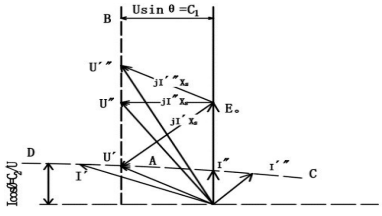

FIGURE 14. Power factor angle adjustment diagram.

For the MTPA control of the surface permanent magnet synchronous motor, it is actually $i_d = 0$ control. The efficiency loop control of the permanent magnet synchronous motor actually achieves the purpose of controlling the power factor angle by adjusting the applied voltage amplitude, so that the power angle is equal to the power factor angle.

$$Q = {}^{3}/_{2}\left(v_\beta^* i_\alpha - v_\alpha^* i_\beta\right) \tag{25}$$

The power factor angle is calculated as:

$$\varphi = \mathrm{a}\tan 2(Q, P) \tag{26}$$

Instantaneous active power is

$$p(t) = \frac{3}{2}R_s I_s^2 + \frac{3}{2}\omega_e\left[\left(\psi_f i_q + \left(L_d - L_q\right) i_d i_q\right)\right] \tag{27}$$

Instantaneous reactive power is

$$q(t) = \frac{3}{2}\omega_e\left[\left(L_d i_d^2 + L_q i_q^2 + \psi_f i_d\right)\right] \tag{28}$$

Available after finishing

$$Q = \frac{3}{2}\omega_e\left[\left(L_s I_s^2 + \psi_f i_d\right)\right] \tag{29}$$

$$i_d = {}^{2Q}/_{3\omega_e\psi_f} - {}^{L_s I_s^2}/_{\psi_f} \tag{30}$$

Figure.15 shows the vector phase diagram for the steady state and transient conditions of the motor. In the figure, a is steady state ($i_d = 0$), at which time the best efficiency control is achieved, b, c is the motor vector in the transient state (in this case, $i_d \neq 0$). By controlling the amplitude of the input voltage, the purpose of controlling the vector current is achieved (Fig. 14), and finally the MTPA control is realized.

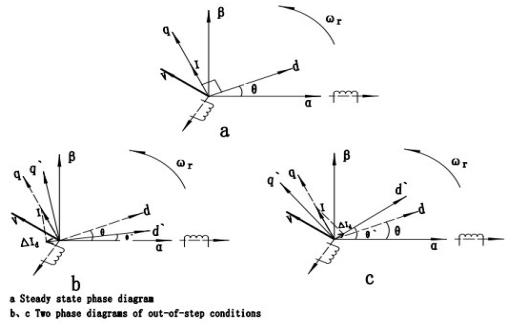

FIGURE 15. MTPA adjustment method.

E. CLOSED LOOP PI PARAMETERS TUNING

The ultimate goal of both V/f closed loops is to stabilize the system, give the system a design similar to the damping link. As can be seen from the above, the adjustment of the two closed loops is actually the adjustment process for ΔT_e.The equivalent small-signal closed-loop adjustment block diagram is shown in Figure 16 and Figure 17.

$$K_\delta = \frac{\partial T_e}{\partial \delta}\,|_{\delta 0} \tag{31}$$

$$K_d = \frac{\Delta I_d}{\Delta P_e} = -\frac{2}{3U_\delta}\cdot\frac{1}{\frac{\partial I}{\partial I_d}|_{I_{d0}}} \tag{32}$$

$$K_v = \frac{\partial T_e}{\partial U_\delta}\,|_{U_{\delta 0}} \tag{33}$$

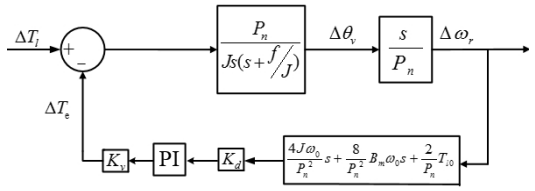

FIGURE 16. Efficiency loop simplifies small signal adjustment block diagram.

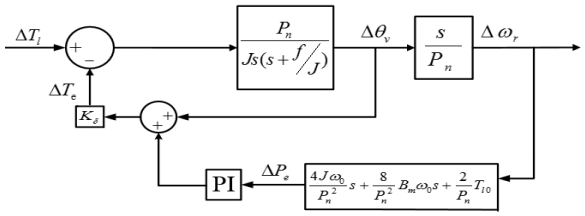

FIGURE 17. Stabilization link simplifies small signal adjustment block diagram.

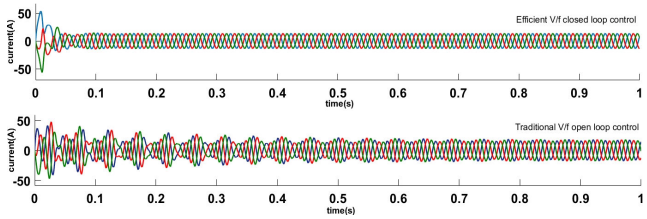

FIGURE 18. Comparison of current under two kinds of V/f control.

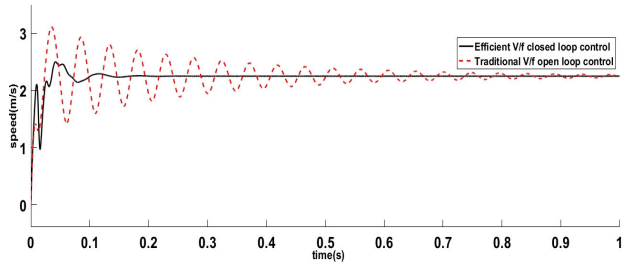

FIGURE 19. Comparison of speeds under two kinds of V/f control.

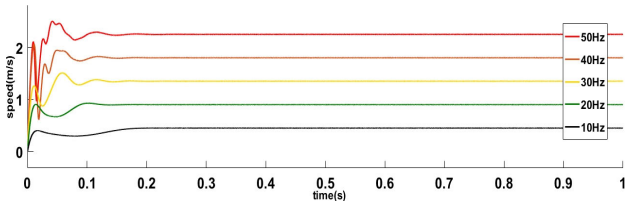

FIGURE 20. Speed comparison under different frequency commands (F_{load} = 1000N).

Two closed-loop systems meet stable conditions by designing two PI controller parameters. Since the amount of calculation is too large, a method such as simplified omission is usually used to obtain a range of estimates, and finally the specific parameter values are determined by performing experiments.

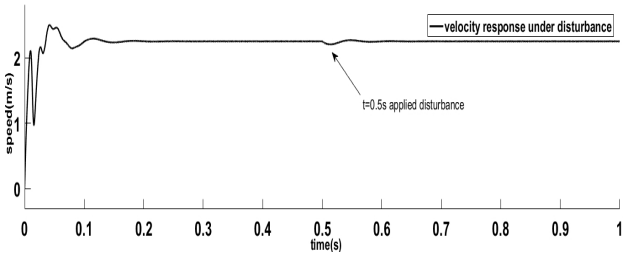

FIGURE 21. Speed response diagram under external disturbance (f = 50hz, F_{load} = 1000N, F_r = 100N).

FIGURE 22. SW-PMLSM industrial hoist prototype.

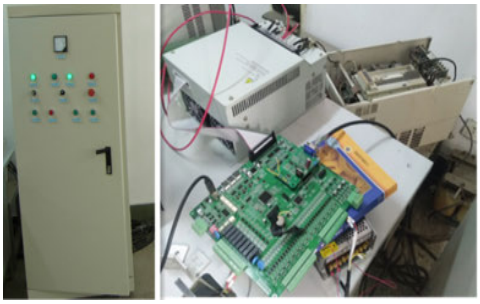

FIGURE 23. SW-PMLSM winding switching control cabinet and motor drive control module.

F. V/F CONTROL SIMULATION ANALYSIS

In order to verify the feasibility of the closed-loop high-efficiency V/f control strategy on SW-PMLSM, a simulation study was carried out on matlab. The simulation uses the V/f control closed-loop high-efficiency control strategy to compare with the traditional open-loop control. The simulation results are shown in the figures below.

As can be seen from figures 18 and 19, the high efficiency V/f has better control performance than the conventional V/f control. It can be concluded from Figure 20 that the high efficiency V/f control has a wider frequency steady state input characteristic. Similarly, Figure 21 demonstrates that the high-efficiency V/f control has strong disturbance recovery capability and is robust.

V. PHYSICAL TEST AND ANALYSIS

In order to further verify the feasibility of the algorithm, an experimental study was carried out in the

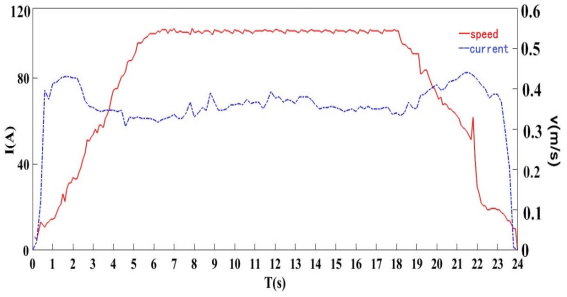

FIGURE 24. Speed and current curve.

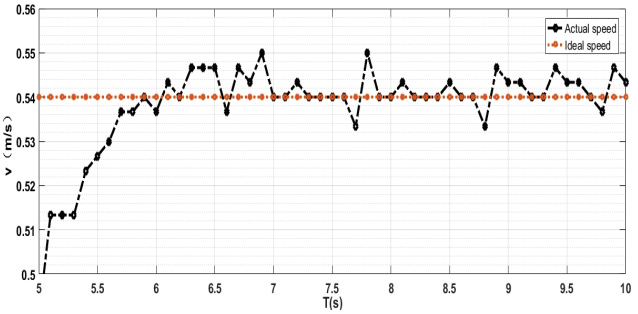

FIGURE 25. Speed dynamics during steady operation.

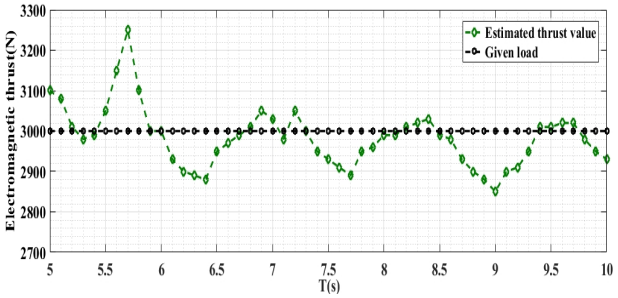

FIGURE 26. Dynamic characteristics of electromagnetic thrust during stable operation.

SW-PMLSM industrial lift prototype system of Henan Polytechnic University. The experimental platform is shown in Figures 22 and 23.

Figure 24 shows the current and velocity dynamics of the SW-PMLSM lifting system at full stroke. In the initial stage, the combination of soft start and inverter makes the running speed of the motor increase steadily. After reaching the ideal speed, it runs stably. In the deceleration phase, the reverse connection of the winding and the brake work together to make the motor speed drop evenly.

Figure 25, 26 show the speed and electromagnetic thrust dynamics of the SW-PMLSM lifting system in the stable operation phase. It can be seen from the figure that the speed and thrust of the system have better dynamic characteristics during the steady lifting process (The electromagnetic thrust is estimated by the formula $F_e = {}^{P_e}/_{v}$).

VI. CONCLUSION

In this paper, the SW-PMLSM rotor side model is established by analyzing the electromagnetic parameters of the motor in each effective segment during the running process of SW-PMLSM. The rotor side model is more helpful in analyzing the trend of electromagnetic force and motion speed. At the same time, through the formula analysis and discussion, it is considered that the segmentation power supply segment vector control can obtain the best control effect. However, due to the limitation of control cost, most industrial-grade controls use a single-supply parallel power supply. Due to the long-stroke motor installation, low-cost V/f control is an optional sensorless sensor control. Finally, an efficient V/f control method is proposed, which not only improves the high-frequency steady-state control problem that traditional V/f control does not have, but also achieves efficiency control, effective control and robustness.

APPENDIX

TABLE 1. Simulated motor parameters.

Symbol	Quantity	Value
ψ_f	Permanent magnet flux linkage	0.655
B	Magnetic flux density,Magnetic induction	$3.035*10^{-4}$
M	Masst	510
P_n	Number of pole pairs	8
R	Winding resistance	7.9
$L_{s\delta}$	Leakage inductance	$1.3*10^{-3}$
L_m	Equivalent magnetizing inductance	$3.9*10^{-2}$
τ	Pole distance	$22.5*10^{-3}$

REFERENCES

[1] S.-G. Lee, S.-A. Kim, S. Saha, Y.-W. Zhu, and Y.-H. Cho, "Optimal structure design for minimizing detent force of PMLSM for a ropeless elevator," *IEEE Trans. Magn.*, vol. 50, no. 1, Jan. 2014, Art. no. 4001104.

[2] M.-M. Koo, J.-Y. Choi, H.-J. Shin, and J.-M. Kim, "No-load analysis of PMLSM with Halbach array and PM overhang based on three-dimensional analytical method," *IEEE Trans. Appl. Supercond.*, vol. 26, no. 4, Jun. 2016, Art. no. 0604905.

[3] C. Yang, T. Ma, Z. Che, and L. Zhou, "An adaptive-gain sliding mode observer for sensorless control of permanent magnet linear synchronous motors," *IEEE Access*, vol. 6, pp. 3469–3478, 2018.

[4] H. Zhang, X. Wang, F. Yu, and Q. Liu, "Characteristics of segment winding permanent magnet linear synchronous motor switching failure," in *Proc. IEEE Int. Conf. Mechtron. Automat.*, Tianjin, China, Aug. 2014, pp. 402–407.

[5] J. Hongr, L. Li, D. Pan, and Z. Zong, "Comparison of two current predictive control methods for a segment winding permanent magnet linear synchronous motor," in *Proc. 16th Int. Symp. Electromagn. Launch Technol.*, Beijing, China, 2012, pp. 1–7.

[6] N. R. Tavana and A. Shoulaie, "Pole-shape optimization of permanent-magnet linear synchronous motor for reduction of thrust ripple," *Energy Convers. Manage.*, vol. 52, pp. 349–354, Jan. 2011.

[7] L. Li-Yi, H. Jun-Jie, W. Hong-Xing, L. Peng, Z. Zhe, and L. Xiao-Peng, "Section crossing drive with fuzzy-PI controller for the long stroke electromagnetic launcher," *IEEE Trans. Magn.*, vol. 45, no. 1, pp. 363–367, Jan. 2009.

[8] K. Suzuki, Y. J. Kim, and H. Dohmeki, "Driving method of permanent-magnet linear synchronous motor with the stationary discontinuous armature for long-distance transportation system," *IEEE Trans. Ind. Electron.*, vol. 59, no. 5, pp. 2227–2235, May 2012.
[9] J. Hong, D. Pan, and Z. Zong, "Comparison of the two current predictive-control methods for a segment-winding permanent-magnet linear synchronous motor," *IEEE Trans. Plasma Sci.*, vol. 41, no. 5, pp. 1167–1173, May 2013.
[10] L. Li, H. Zhu, and C. C. Chan, "Investigation of the inter-stator current control for long primary winding segmented PMLSM used in electromagnetic launch system," in *Proc. 17th Int. Symp. Electromagn. Launch Technol.*, La Jolla, CA, USA, Jul. 2014, pp. 1–6.
[11] L. Li, H. Zhu, M. Ma, and Q. Chen, "Proposal of the sensorless control method of long primary segmented PMLSM applied in electromagnetic catapult," in *Proc. 16th Int. Symp. Electromagn. Launch Technol.*, Beijing, China, May 2012, pp. 1–6.
[12] M. N. Ma and L. Y. Li, "Modeling and flux leakage analysis for long-stator PM linear motor including longitudinal end effects," in *Proc. IEEE Int. Conf. Appl. Supercond. Electromagn. Devices (ASEMD)*, Shanghai, China, Nov. 2015, pp. 494–495.
[13] X. Wang, H. Feng, B. Xu, and X. Xu, "Research on permanent magnet linear synchronous motor for Rope-less hoist system," *J. Comput.*, vol. 7, no. 6, pp. 1361–1368, 2012.
[14] X. Wang, Z. Zhang, X. Xu, and Y. Cui, "Influence of using conditions on the performance of PM linear synchronous motor for ropeless elevator," in *Proc. Int. Conf. Electr. Mach. Syst.*, Aug. 2011, pp. 1–5.
[15] Z. Hongwei, W. Xinhuan, and Y. Fashan, "Research on the operation control for rope-less hoist system driven by permanent magnet linear synchronous motor," in *Proc. 31st Chin. Control Conf.*, Jul. 2012, pp. 5619–5624.
[16] S. Xuanfeng, L. Qingfu, and Y. Shiying, "Integrated modeling and simulation of the systems driven by multi-segment primary permanent linear synchronous motors," *Trans. China Electrotech. Soc.*, vol. 21, pp. 52–57, Mar. 2006.
[17] S. Xuanfeng, L. Qingfu, Y. Shiying, and J. Liucheng, "Analysis on running process of permanent linear synchronous motors with discontinuous stators," *J. Xi'an Jiaotong Univ.*, vol. 38, pp. 1292–1295 and 1300, Dec. 2004.
[18] Q. Jiang and Q. Lu, "Performance investigation of a five-phase multi-segment primary PMLSM for ropeless elevator," in *Proc. IEEE Int. Magn. Conf. (INTERMAG)*, Singapore, Apr. 2018, p. 1.
[19] J.-I. Itoh, N. Nomura, and H. Ohsawa, "A comparison between V/f control and position-sensorless vector control for the permanent magnet synchronous motor," in *Proc. Power Convers. Conf.*, Apr. 2002, pp. 1310–1315.
[20] A. Moldovan, F. Blaabjerg, and I. Boldea, "Active-flux-based, V/f-with-stabilizing-loops versus sensorless vector control of IPMSM Drives," in *Proc. Int. Symp. Ind. Electron.*, Jun. 2011, pp. 27–30.
[21] Z. Tang, X. Li, S. Dusmez, and B. Akin, "A new V/f-based sensorless MTPA control for IPMSM drives," *IEEE Trans. Power Electronics.*, vol. 31, no. 6, pp. 4400–4415, Jun. 2016.
[22] Z. Tang and B. Akin, "A robust V/f based sensorless MTPA control strategy for IPM drives," in *Proc. IEEE Appl. Power Electron. Conf. Expo. (APEC)*, Mar. 2015, pp. 1575–1581.
[23] S. H. Jafari, K. A. Corzine, and J. Huang, "Efficiency optimization of a sensorless V/f control method for PMSM," in *Proc. 3rd IEEE Int. Symp. Sensorless Control Elect. Drives (SLED)*, Sep. 2012, pp. 1–5.
[24] G.-D. Andreescu, C.-E. Coman, A. Moldovan, and I. Boldea, "Stable V/f control system with unity power factor for PMSM drives," in *Proc. 13th Int. Conf. Optim. Elect. Electron. Equip. (OPTIM)*, May 2012, pp. 432–438.

LEILEI CUI received the B.Eng. degree in electrical engineering and automation from Henan Polytechnic University, Jiaozuo, China, in 2013, where he is currently pursuing the M.Eng. degree. His research interests include control technology for permanent magnet linear synchronous motor and industrial process control.

HONGWEI ZHANG received the B.Eng. degree from the Jiaozuo Institute of Technology, in 2002, and the M.Eng. and Ph.D. degrees from Henan Polytechnic University, in 2005 and 2015, respectively, where he is currently an Associate Professor. His main research interests include motion system control and industrial process control.

DI JIANG received the B.Eng. degree in electrical engineering and automation from Henan Polytechnic University, Jiaozuo, China, in 2017, where he is currently pursuing the M.Eng. degree.

His research interest includes control technology for permanent magnet linear synchronous motor.